Medicago truncatula ABCG40 is a cytokinin importer negatively regulating lateral root density and nodule number

Tomasz Jamruszka[1], Joanna Banasiak[1,2], Aleksandra Pawela[1], Karolina Jarzyniak[1,2], Jian Xia[3], Wanda Biała-Leonhard[1], Lenka Plačková[4], Francesca Romana Iacobini[3], Ondřej Novák[4], Markus Geisler[3], Michał Jasiński[1,2] *

1. Department of Plant Molecular Physiology, Institute of Bioorganic Chemistry, Polish Academy of Sciences, Z. Noskowskiego 12/14, 61-704 Poznań, Poland
2. Department of Biochemistry and Biotechnology, Poznań University of Life Sciences, Dojazd 11, 60-632 Poznań, Poland.
3. Department of Biology, University of Fribourg, Chemin du Musée 10, CH-1700 Fribourg, Switzerland
4. Laboratory of Growth Regulators, Faculty of Science, Palacký University and Institute of Experimental Botany, The Czech Academy of Sciences, Šlechtitelů 27, CZ-78371, Olomouc, Czech Republic

* For correspondence Michał Jasiński, Department of Plant Molecular Physiology, Institute of Bioorganic Chemistry, Polish Academy of Sciences, Z. Noskowskiego 12/14, 61-704 Poznań, Poland, (+48) 61 852 85 03, (e-mail jasinski@ibch.poznan.pl)

The author responsible for distribution of materials integral to the findings presented in this article in accordance with the policy described in the Instructions for Authors (https://academic.oup.com/plcell/pages/General-Instructions) is: Michał Jasiński (jasinski@ibch.poznan.pl).

Short title: CK importer affects root morphology

Key words: ABCG transporters, cytokinin, root morphology, nodulation, lateral root, root apical meristem

ORCID IDs
Tomasz Jamruszka: 0000-0003-4445-5624
Joanna Banasiak: 0000-0002-2834-7116

35 Aleksandra Pawela: 0000-0001-5017-4912
36 Karolina Jarzyniak: 0000-0002-9535-7306
37 Jian Xia: 0000-0001-9294-7960
38 Wanda Biała-Leonhard: 0000-0001-8594-2846
39 Lenka Plačková: 0000-0003-2537-4933
40 Francesca Romana Iacobini: 0000-0001-8339-6909
41 Ondřej Novák: 0000-0003-3452-0154
42 Markus Geisler: 0000-0002-6641-5810
43 Michał Jasiński: 0000-0003-0904-5873
44
45

ABSTRACT

Numerous studies suggest a relevant role of cytokinin (CK) distribution in shaping of plant morphology upon changing environment. Nonetheless, our knowledge about an involvement of short-distance CK translocation in root mineral nutrition is still scarce and specific role of CK transporters in root morphology has yet to be established. Revealing the molecular identity of CK transporters is thereby crucial for better understanding of root plasticity during soil fertility, as well as more frequently encountered plant nutrients deficiencies. In this work, we identified and characterized the *Medicago truncatula* full-size ATP-binding cassette (ABC) transporter belonging to the G subfamily, namely MtABCG40 as a CK importer. Its expression is root-specific and is induced by nitrogen deprivation and CKs. Our analyses indicate that MtABCG40 has a negative impact on lateral root density through decreased lateral root initiation and enhancement of primary root elongation. Moreover, in line with postulated resemblance to lateral roots, we also observed an inhibitory influence of this transporter on nodule number. Our results suggest that MtABCG40 action affects CK signaling which impacts on the cellular response to auxin. We present data that demonstrate a full-size ABCG transporter with a novel function in legumes and CK transport.

INTRODUCTION

Plant roots show high plasticity to meet the needs during fluctuations of nitrogen availability in the soil and can adapt both their physiology and morphology, accordingly. Changes of root physiology are controlled by the production and translocation of various signaling molecules. Those include phytohormones, such as cytokinins (CKs), that can have local effects or trigger a systemic response. Both alter root morphology together with nitrogen uptake from the soil (Jia and von Wiren, 2020). Adjustment of the primary root length and lateral root number, manifested often by changes in lateral root density, are two of the plant reactions to varying nitrogen concentrations (Lopez-Bucio et al., 2003; Lima et al., 2010; Postma et al., 2014). An increase of the distance between adjacent lateral roots, called lateral root spacing, is triggered by different factors, especially CKs, which suppress a positive effect of auxin on lateral root initiation (Laplaze et al., 2007). The spacing results also from CKs influence on the root apical meristem (RAM), decreasing its size thus decelerating root growth (Dello Ioio et al., 2007; Dello Ioio et al., 2008). In legumes, a change in root morphology during nitrogen deficiency can also result from an interaction with symbiotic partners, namely nitrogen-fixing soil bacteria collectively called rhizobia. The latter induce cortical cell divisions to form root nodules (Oldroyd et al., 2011). Notably, CKs in legumes control the initial steps of nodule formation by

promoting cell proliferation in the cortex giving rise to nodule primordia (Gonzalez-Rizzo et al., 2006; Murray et al., 2007). However, they can act also as negative regulators of nodulation by inhibition of further infections in the epidermis (Miri et al., 2019) and systemic suppression of primordium formation (Sasaki et al., 2014). Of note, CK action in lateral root and nodule organogenesis is highly dependent on plant nitrogen status (Gu et al., 2018).

Aliphatic CKs are adenine derivatives with isoprenoid substitutions at the N^6 position. Ribosides, their biologically inactive forms, feature more complex structures with an additional ribose moiety, and are translocated along the plant within vascular tissues (Kieber and Schaller, 2014; Osugi et al., 2017). The cleavage of the sugar component from CK riboside 5'-monophosphates by LONELY GUY (LOG) enzymes leads to the formation of their active forms, isopentenyladenine (iP) or *trans*-zeatin (*tZ*) (Kurakawa et al., 2007). To trigger specific outcomes, CKs have to be translocated across biological membranes and perceived, either intracellularly or extracellularly (Romanov et al., 2018).

Up to date, several CK transporters with functions in roots have been described. Three of them, namely MtABCG56, AtABCG14, and OsABCG18, belong to the G subfamily of ATP-BINDING CASSETTE (ABC) family of transporters (Ko et al., 2014; Zhang et al., 2014; Zhao et al., 2019; Jarzyniak et al., 2021). ABCG transporters in general translocate molecules (both as an exporters and importers) across biological membranes using ATP as a source of energy. Their action has been assigned to different developmental processes, reactions to abiotic stresses, interactions with pathogens, and symbiotic associations (Lefevre and Boutry, 2018). These also involve translocation of other phytohormones, like strigolactones (Kretzschmar et al., 2012; Banasiak et al., 2020) and abscisic acid (ABA) (Kang et al., 2010; Pawela et al., 2019). To date, the only CK transporter implicated in nodulation, MtABCG56, is localized to the plasma membrane (PM) and transports *tZ* as well as iP. MtABCG56 exports CK from rhizodermal and cortical cells after perception of symbiotic bacteria-derived Nod factors in the root susceptible zone (Jarzyniak et al., 2021). On the other hand, *ABCG14* from non-symbiotic *A. thaliana* is expressed mainly in the pericycle and vasculature of the root along with CK biosynthesis genes, like *ISOPENTENYLTRANSFERASE 3 (IPT3)* and *CYTOCHROME P450 (CYP) MONOOXYGENASES*. AtABCG14 is a PM *tZ*-type CK efflux pump, which contributes to their long-distance translocation throughout xylem and subsequent systemic impact on plant development (Ko et al., 2014; Zhang et al., 2014). Notably, a similar function was later demonstrated for its ortholog from *Oryza sativa*, OsABCG8 (Zhao et al., 2019).

Other CK transporters known to function in roots belong to the PURINE PERMEASE (PUP), AZA-GUANINE RESISTANCE (AZG) and EQUILIBRATIVE NUCLEOSIDE

TRANSPORTER (ENT) families. AtPUP14 is a PM importer of bioactive CKs (*tZ*, iP and 6-benzylaminopurine 6-BAP) in Arabidopsis seedlings, specifically in their root tip meristematic cells and lateral root primordia. PUP14 action creates a sink for CKs inside the cell that the hormone can no longer be perceived in the apoplast by PM-bound receptors and trigger a specific cell response. Loss of PUP14 transport activity leads to root morphological defects (Zurcher et al., 2016). AtAZG2, which localizes to the PM and endoplasmic reticulum (ER) of root cells, transports iP, *tZ*, 6-BAP and kinetin. *AtAZG2* is expressed in tissues overlaying lateral root primordia and, as opposed to auxin, negatively influences lateral root emergence (Tessi et al., 2021). Finally, AtENT3 translocates CK nucleotides through the PMs of root vascular bundles and in the root tip, enabling systemic movement of the hormone throughout the plant, affecting its development (Traub et al., 2007; Cornelius et al., 2012; Korobova et al., 2021).

Here we identify and characterize the *Medicago truncatula* full-size ABCG transporter, MtABCG40, as a CK importer. *MtABCG40* expression is root-specific and is induced by nitrogen deprivation and CKs. Our analyses indicate that MtABCG40 has a negative impact on lateral root density through decreased lateral root initiation and enhancement of primary root elongation. Moreover, lack of this transporter leads to increased nodule number. Our results suggest that MtABCG40 action affects CK signaling which impacts on the cellular response to auxin.

RESULTS

Lateral root density is negatively regulated by MtABCG40 in response to environmental and internal cues

MtABCG40 (*Medtr7g098300*) encodes a full-size ABC transporter belonging to a legume-specific clade of the G subfamily (Banasiak and Jasiński, 2014; Jarzyniak et al., 2021). High expression of *MtABCG40* in the root prompted us to determine a possible role of the encoded transporter in this organ (Figure 1A). Due to a reported multifaceted influence of environmental stimuli, such as nutrients and, in particular, nitrogen status, on root morphology, we investigated *MtABCG40* expression at different concentrations of ammonium nitrate (NH_4NO_3). We noted that plants grown on solid media not supplemented with nitrogen (here referred to as 0 mM NH_4NO_3) exhibited the highest *MtABCG40* expression and the lowest lateral root density, compared to media with added NH_4NO_3 (Figure 1B). The decline in the lateral root density, resulting from an enlargement of a spacing between adjacent lateral roots, was a consequence

of an acceleration of primary root elongation, and to a lesser extent of a decrease in the lateral root number (Supplemental Figure S1). We also investigated a possible relation between the *MtABCG40* expression and lateral root density upon treatment with hormones known to trigger changes in root architecture, such as ABA and CKs. *MtABCG40* mRNA abundance decreased after ABA treatment which was associated with increased lateral root density, while application of 6-BAP, a synthetic CK, resulted in an induction of *MtABCG40* expression accompanied by a decline in lateral root density (Figure 1, C and D).

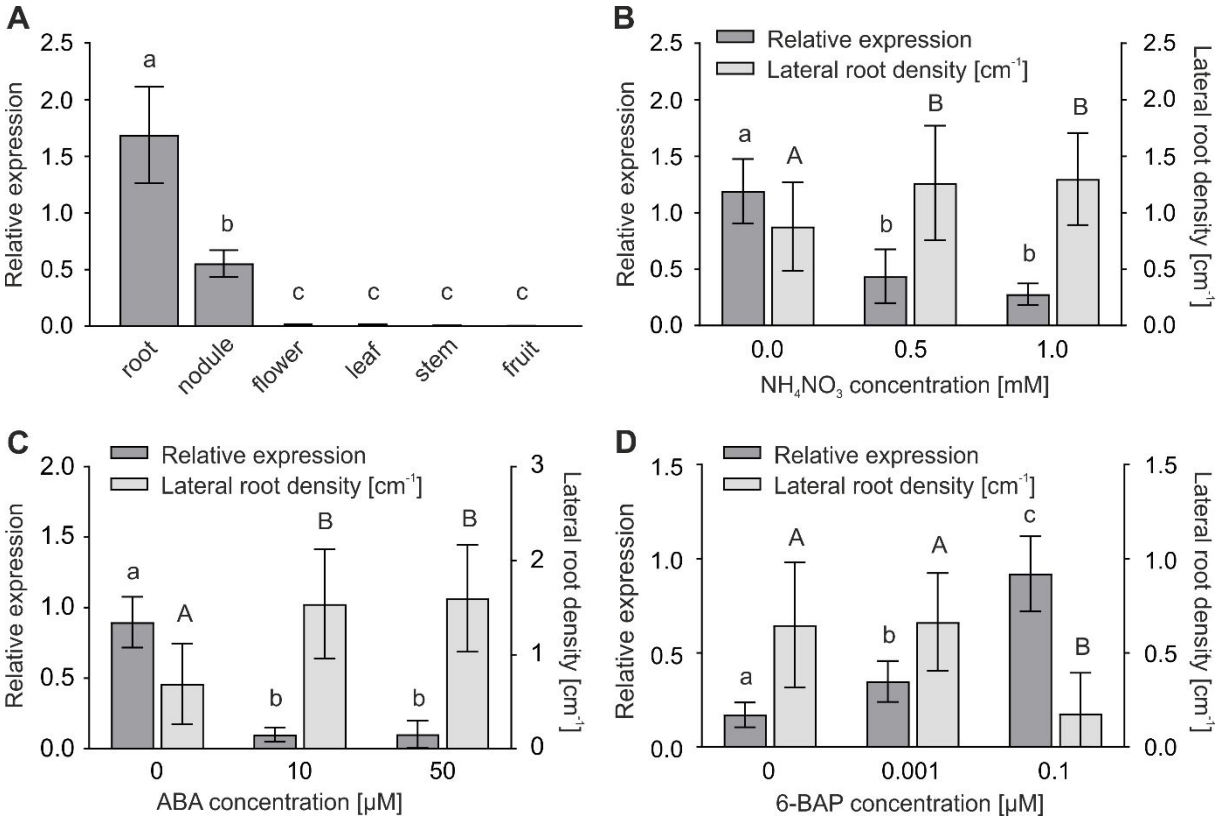

Figure 1. A negative relationship exists between *MtABCG40* expression and lateral root density. A, *MtABCG40* transcripts were detected only in roots and nodules. B-D, Expression of *MtABCG40* and lateral root density at different concentrations of ammonium nitrate (NH_4NO_3) (B), abscisic acid (ABA) (C), and 6-benzylaminopurine (6-BAP) (D). Transcript levels were measured by quantitative real-time PCR and normalized to *actin*. Expression data represent the mean ± SD of three independent biological experiments and two or three technical repeats. Identical or different lowercase letters indicate no or significant differences in the expression, respectively; $P < 0.05$ (A-D). Significant differences from the control plants determined by the one-way ANOVA with a post hoc Tukey's multiple comparison test (A, B and D), Kruskal-Wallis test with a post hoc Dunn's multiple comparison test (C). The lateral root density data represent the mean ± SD of 3 independent biological experiments (31-69 roots per condition). Identical or different uppercase letters indicate no or significant differences in the lateral root density, respectively; $P < 0.05$ (B-D). Significant differences from the control plants determined by the one-way ANOVA with a post hoc Tukey's multiple comparison test (B), Kruskal–Wallis test with a post hoc Dunn's multiple comparison test (C and D).

Two *M. truncatula* lines with tobacco retrotransposon (*Tnt1*) insertions in the 22nd exon (NF21323, *mtabcg40-1*) and first intron (NF17891, *mtabcg40-2*) of *MtABCG40* were identified (Supplemental Figure S2). When grown on nitrogen-depleted media, the mutants, in comparison to WT plants, exhibited a significant increase in lateral root density, which could indicate a negative influence of *MtABCG40* on this trait (Figure 2A). The phenotype was due to a reduction in the root length (Figure 2B) and an increase in the lateral root number (Figure 2C). Notably, observed differences were less pronounced when nitrogen was present in the media (1 mM NH_4NO_3) (Supplemental Figure S3).

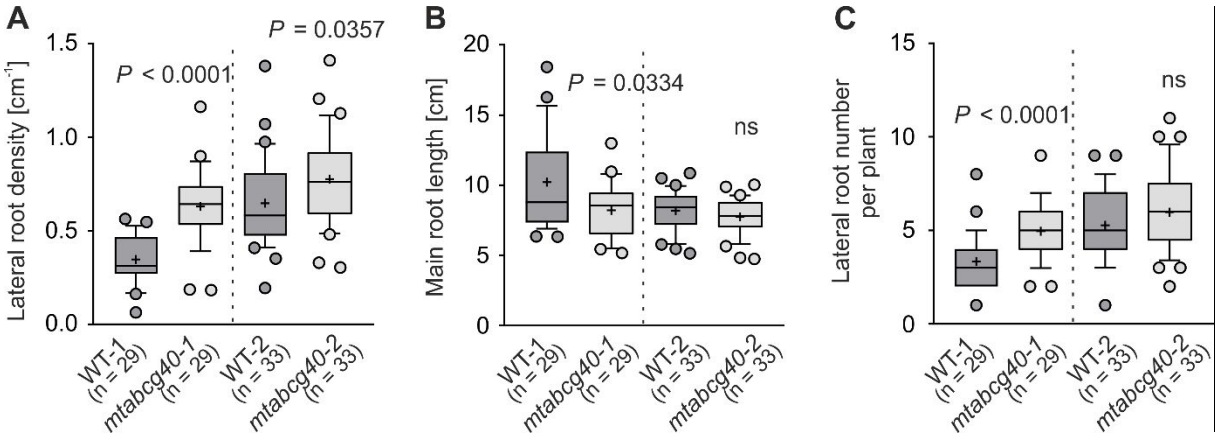

Figure 2. Mutation of *MtABCG40* increases lateral root density by reducing the primary root length and promoting lateral root formation. Lateral root density (A), primary root length (B), and lateral root number (C) in control (WT) and mutant (*mtabcg40*) plants. For each box-and-whiskers plot: the central black line represents the median; '+' represents the mean; the box extends from the 25th to 75th percentiles; the whiskers are drawn down to the 10th percentile and up to the 90th. Points below and above the whiskers are drawn as individual dots. Significant differences from the control plants determined by two-tailed Student's t-test with Welch correction (A), two-tailed Mann–Whitney test (B and C); ns, not significant; n represents the number of individual plants obtained from three independent biological experiments (A-C).

MtABCG40 is a plasma membrane cytokinin importer

Since 6-BAP treatment induced *MtABCG40* expression (Figure 1D), and given its close phylogenetic relationship to the previously described CK transporter, MtABCG56 (Supplemental Figure S4) (Jarzyniak et al., 2021), we decided to study the possible role of MtABCG40 in CK translocation. Initially, in addition to 6-BAP, we tested the effect of other CKs on the *MtABCG40* expression, and observed that the biologically active CKs, iP and *tZ*, induced *MtABCG40* mRNA accumulation in roots (Figure 3, A and B).

To demonstrate the direct involvement of MtABCG40 in the translocation of CKs, transport experiments with ^{14}C-labelled *tZ* were carried out. First, we expressed *GFP-MtABCG40* under the control of the *AtUBI10* promoter in tobacco protoplasts using

Agrobacterium-mediated leaf infiltration and showed the PM localization of MtABCG40 (Figure 3C). Subsequently, protoplasts isolated from the transformed leaves were loaded with ^{14}C-*t*Z and *t*Z export was determined by separating protoplasts from supernatants. Protoplasts expressing *GFP-MtABCG40* exported less ^{14}C-*t*Z than the vector control (Figure 3D). ^{14}C-*t*Z export catalyzed by GFP-MtABCG40 was specific as the diffusion control, auxin (indole-3-acetic acid, IAA), known to be transported by some members of ABC family (Geisler et al., 2005), was not affected by expression of *GFP-MtABCG40* (Figure 3E). Reduced ^{14}C-*t*Z export together with a PM localization suggests GFP-MtABCG40 plays a role in the net import of CKs. In order to further investigate its potential role in CK import, we conducted ^{14}C-*t*Z uptake experiments in protoplasts transformed with *AtUBI10:GFP-MtABCG40.* As expected, *AtUBI10:GFP-MtABCG40* protoplasts imported significantly more ^{14}C-*t*Z than the vector control, which had negative import rates (ie. net uptake) that was most likely due to endogenous *t*Z export systems present in tobacco protoplasts (Figure 3F). In summary, our data suggest that MtABCG40 functions as a PM importer of the active CK, *t*Z.

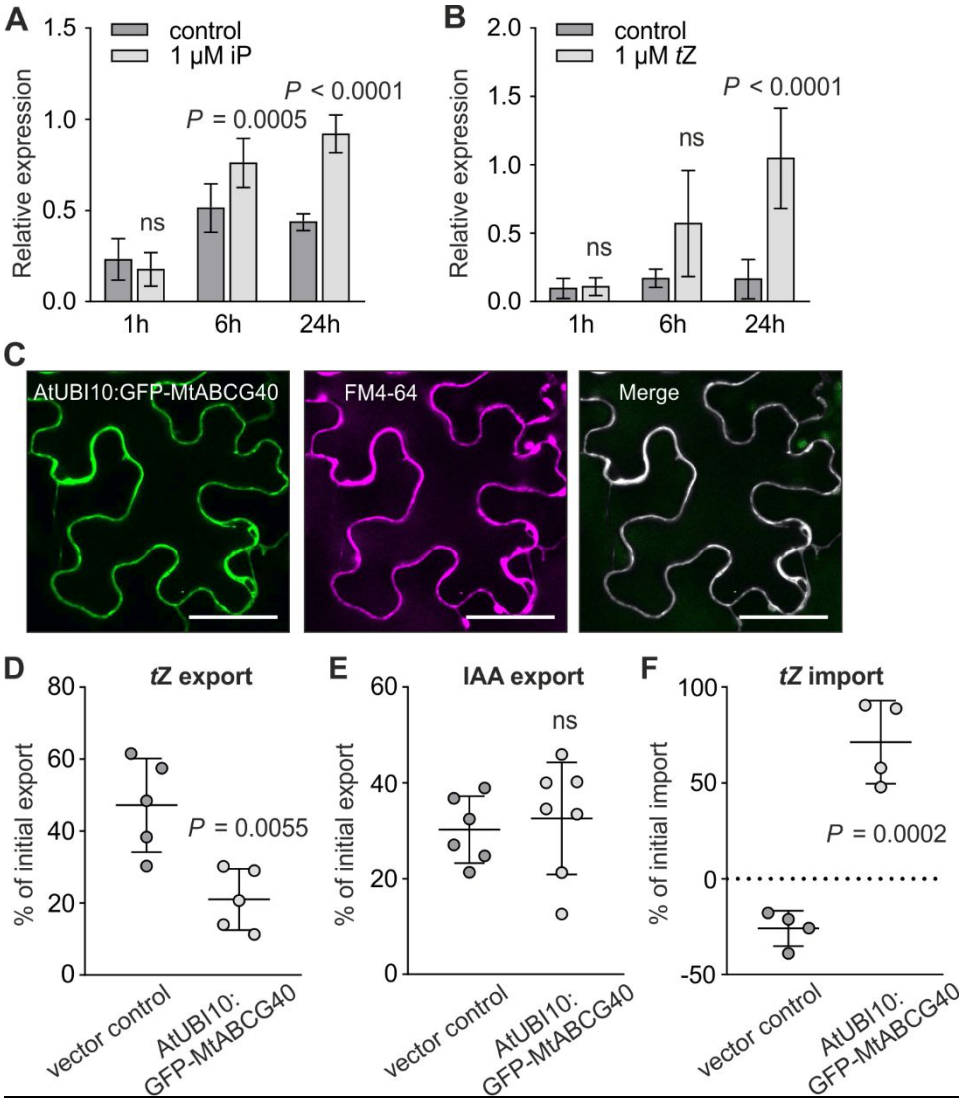

Figure 3. MtABCG40 is a plasma membrane (PM) cytokinin (CK) importer. A and B, *MtABCG40* expression profile upon CK treatment. Transcript levels of roots mock-treated or treated with 1 µM isopentenyladenine (iP) (A), and 1 µM *trans*-zeatin (*t*Z) (B), measured by quantitative real-time PCR and normalized to *actin* from *Medicago truncatula*. Data represent the mean ± SD of three independent biological experiments and three technical repeats. Significant differences from the mock-treated plants determined by two-tailed Student's t-test with Welch correction (A and B). C, PM localization of the GFP-MtABCG40 fusion protein in Agrobacterium-infiltrated *Nicotiana benthamiana* leaf epidermal cells with the PM marker dye, FM4-64 (Pearson's correlation coefficient, 0.75 ± 0.11). GFP and FM4-64 images were pseudo-coloured in green and magenta, respectively. Scale bars: 50 µm. D-F, Transport experiments in tobacco protoplasts expressing *AtUBI10:GFP-MtABCG40*. [^{14}C]*t*Z (D) and [^{3}H]indole-3-acetic acid ([^{3}H]IAA) (E) export experiments from tobacco protoplasts, as well as [^{14}C]*t*Z import experiments into tobacco protoplasts (F). Data represent the means ± SD from a minimum of 4 independent experiments (transfections). Significant differences from the vector control were determined by two-tailed Student's t-test (D-F).

MtLOG3 activity affects Medicago root morphology upon nitrogen depletion

The formation of active CKs is carried out through a cleavage of the sugar component from their monophosphate riboside forms by LOG enzymes (Kurakawa et al., 2007). Therefore, we

239 investigated a possible relationship between the *MtABCG40* and *MtLOG* and *MtLOG-like* genes
240 under various NH_4NO_3 concentrations. We found that five of these genes, namely *MtLOG2*
241 (*Medtr1g064260*), *MtLOG3* (*Medtr1g057020*), *MtLOG-like 1* (*Medtr1g015830*), *MtLOG-like*
242 *3* (*Medtr3g113710*) and *MtLOG-like 4* (*Medtr4g058740*) (Mortier et al., 2014; van Zeijl et al.,
243 2015) showed increased expression under nitrogen depletion, which also positively influenced
244 the level of *MtABCG40* mRNA (Figure 4A). We then focused our attention on the most strongly
245 induced *LOG* gene, *MtLOG3* (van Zeijl et al., 2015), which is the closest homologue of *AtLOG7*
246 (*AT5G06300*), a nitrogen starvation-induced gene with expression in lateral root-forming
247 pericycle cells (Supplemental Figure S5) (Bargmann et al., 2013; Walker et al., 2017). Silencing
248 of *MtLOG3* expression caused an increase in lateral root density (Figure 4B and Supplemental
249 Figure S6) similar to what was observed for *MtABCG40* RNAi-silenced roots (Figure 4B and
250 Supplemental Figure S6) and *mtabcg40* mutants (Figure 2A). This observation prompted us to
251 investigate the *MtABCG40* and *MtLOG3* spatial expression pattern in roots. In order to do this,
252 we generated *M. truncatula* composite plants which contained *MtABCG40* and *MtLOG3*
253 promoters expressing either nuclear-localized versions of green fluorescent protein
254 (*ProMtABCG40:NLS-GFP*), or tdTomato (*ProMtLOG3:NLS-tdTomato*), and *β-glucuronidase*
255 (*ProMtABCG40:GUS* and *ProMtLOG3:GUS*) reporter genes. Transgenic roots subjected to
256 nitrogen deficiency for three weeks revealed that *MtABCG40* expresses mainly in the root
257 vascular tissue, a site of radial, short-distance CK translocation (Ko et al., 2014; Aubry et al.,
258 2019), as well as in the pericycle, endodermis and, less often, in the inner cortex, layers known
259 to be involved in initial cell divisions during lateral root primordium formation in *M. truncatula*
260 (Herrbach et al., 2014). *MtABCG40* expression was also seen in the RAM and lateral root
261 primordium (Figure 4C), where CKs influence meristem size and consequently organ
262 elongation (Dello Ioio et al., 2007). In the same conditions, *MtLOG3* expression overlapped
263 with that of *MtABCG40* in the root stele and lateral root primordium, but only bordered the
264 regions where *MtABCG40* was expressed in the root cap (Figure 4D), a place of CK
265 biosynthesis (Aloni et al., 2005).

266

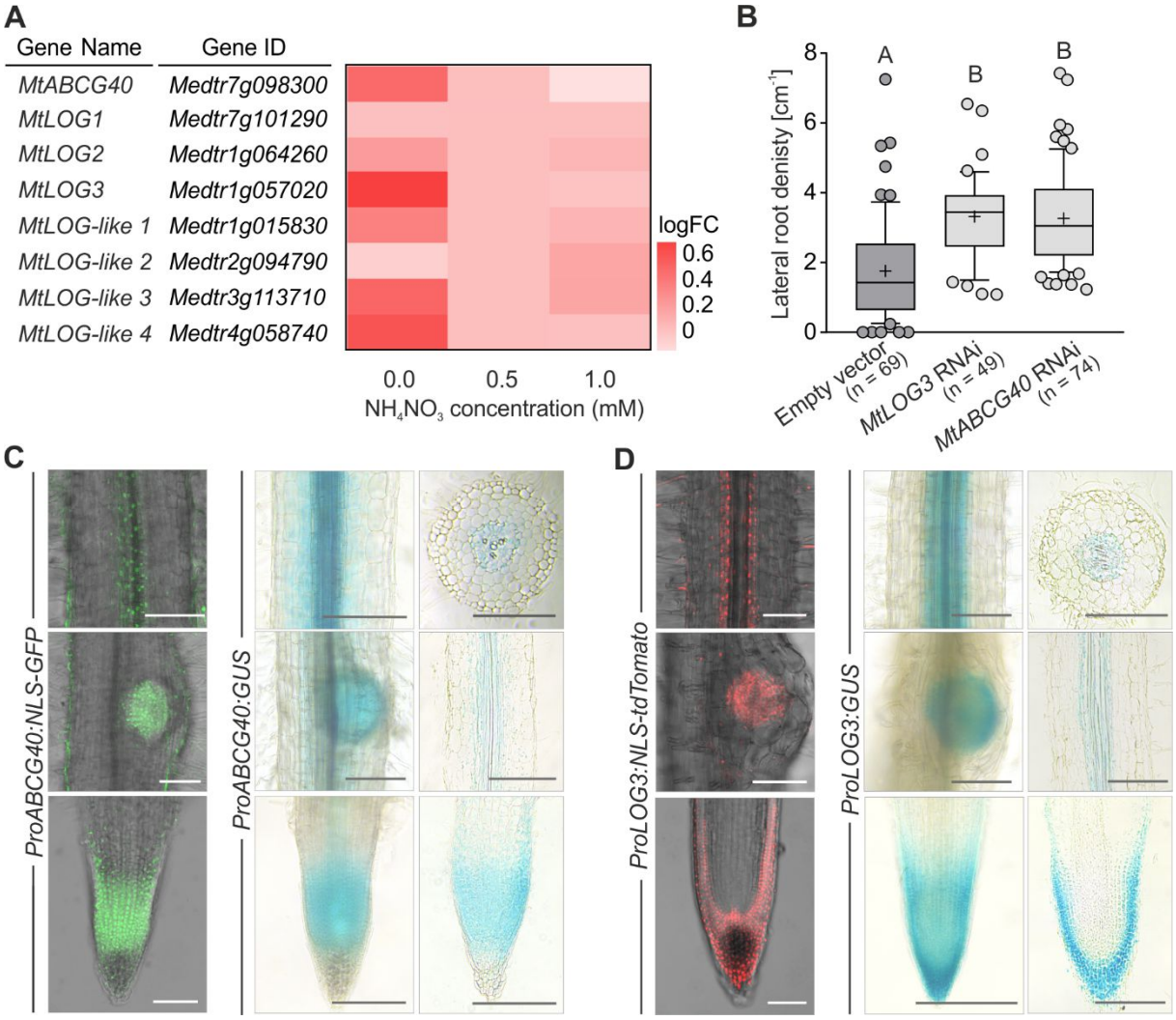

Figure 4. MtABCG40 and MtLOG3 regulate root architecture upon nitrogen starvation. A, Heat map showing the expression of *MtABCG40*, *MtLOG and MtLOG-like* genes in root samples across NH_4NO_3 concentration. Expression is shown as log2 fold changes. B, Lateral root density of *MtLOG3* or *MtABCG40* RNAi-silenced hairy roots in comparison to the empty vector (EV)-transformed control. For each box-and-whiskers plot: the central black line represents the median; '+' represents the mean; the box extends from the 25th to 75th percentiles; the whiskers are drawn down to the 10th percentile and up to the 90th. Points below and above the whiskers are drawn as individual dots. Identical or different uppercase letters indicate no or significant differences in lateral root density, respectively; $P < 0.05$. Significant differences from the EV-transformed control determined by Kruskal-Wallis test with a post hoc Dunn's multiple comparison test; n represents the number of individual roots obtained from three independent biological experiments. C-D, Tissue-specific expression of *MtABCG40* (C) and *MtLOG3* (D) in transgenic roots carrying the *ProMtABCG40:GUS*, *ProMtABCG40:NLS-GFP* and *ProMtLOG3:GUS*, *ProMtLOG3:NLS-tdTomato* constructs, respectively. Each panel contains images from confocal microscopy (left side) and light microscopy with intact roots and cross-sections (right side), including a lateral root primordium and the root apical meristem (RAM). The images are representative of n > 20 roots from three independent experiments (transformations).

Cytokinin response in the root apical meristem is inhibited by MtABCG40

It is well documented that CKs decrease the size of RAM (Dello Ioio et al., 2007; Dello Ioio et al., 2008). To explain the changes in root length between WT and *mtabcg40* plants (Figure 2B),

we analyzed the sizes of their RAM as the distance between the quiescent center (QC) and the transition zone (TZ). The *mtabcg40* mutants exhibited shorter RAMs compared to WT (Figures 5, A and B). Additionally, the negative role of MtABCG40 in CK responses in the root tip was demonstrated by the higher expression of *MtRR4*, a type-A CK response regulator (Gonzalez-Rizzo et al., 2006), in the root meristem of *mtabcg40-1* compared to the control (Figure 5C). Notably, there was no difference in the overall active CK content within those RAMs (Figure 5D), suggesting that the distribution of active CKs rather than their total concentration is affected by loss of *MtABCG40*. Bearing in mind that CKs often antagonize auxin outcomes in meristematic regions, we measured the amount of auxin (IAA) in the RAMs of *mtabcg40* lines and observed its increased level compared to the control (Figure 5E). Moreover, we observed an upregulation of the *DR5* auxin-response reporter in RAMs of *MtABCG40* RNAi-silenced roots (Figure 5F).

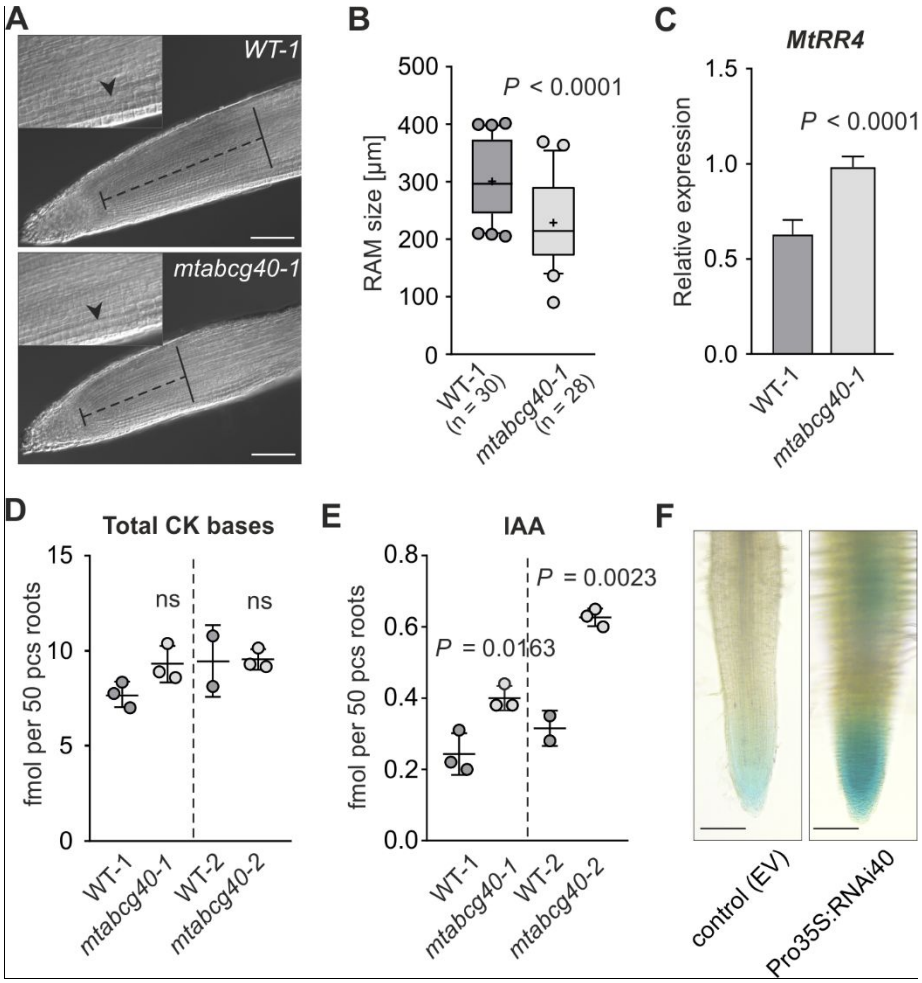

Figure 5. Mutation of *MtABCG40* reduces the size of the *Medicago truncatula* root apical meristem (RAM) upon nitrogen deficiency. A and B, Comparison of the size of RAM between WT-1 and *mtabcg40-1* mutant. Nomarski image of the RAM and apical region of the elongation/differentiation zone (EDZ) of a primary root 10 days after germination (dag). The size of the RAM (black dotted line) was determined as the distance from the quiescent center (QC) to the EDZ. The apical border of the EDZ was defined by the first elongated cortical cell of the second cortical layer (arrowhead) (A). Graph showing the RAM size of *mtabcg40-1* mutant and WT-1. For each box-and-whiskers plot: the central black line represents the median; '+' represents the mean; the box extends from the 25th to 75th percentiles; the whiskers are drawn down to the 10th percentile and up to the 90th. Points below and above the whiskers are drawn as individual dots; n represents the number of analyzed RAMs (B). C and D, Assessment of the level of CK response and cytokinin (CK) bases (*trans*-zeatin, *cis*-zeatin, isopentenyladenine, dihydrozeatin) in RAMs of WT-1 and *mtabcg40-1* mutant. Expression analysis of *MtRR4*, a type-A response regulator, in *mtabcg40-1* and WT-1. Transcript levels were measured by quantitative real-time PCR and normalized to *actin* (C). CK concentration in *mtabcg40-1* and WT-1 (D). E and F, Assessment of auxin (indole-3-acetic acid, IAA) level and response in RAMs of WT-1 and the *mtabcg40-1* mutant. IAA concentration in *mtabcg40-1* and WT-1 (E). *DR5:GUS* reporter expression in *MtABCG40* RNAi-silenced and control (EV) roots, representative images from 10 roots of each construct (F). Data represent the mean ± SD of two independent biological experiments (B), three independent biological experiments and three technical repeats (C), and two or three biological replicates (D and E). Significant differences from the control plants determined by two-tailed Student's t-test (B-E); ns, not significant.

Initial cell divisions in lateral root formation are enhanced in *mtabcg40* plants

To further explore the phenomenon of increased lateral root number in *mtabcg40* plants (Figure 2C), we used gravitropic stimulation of lateral root initiation (Supplemental Figure S7) combined with an EdU (5-ethynyl-2′-deoxyuridine)-staining of DNA in dividing cells (Schiessl et al., 2019). We observed a higher number of cells in lateral root primordia forming on 12-hour gravistimulated roots on *mtabcg40-1* plants compared to control plants (Figure 6, A and B). Since CKs antagonize an auxin-dependent initiation of early cell divisions during lateral root primordium formation (Laplaze et al., 2007), we decided to assess a possible influence of *MtABCG40* on auxin response. We initially examined the expression of *MtABCG40* upon auxin (IAA) treatment and observed its repression (Figure 6C). Furthermore, by using once again gravitropic stimulation of lateral root initiation, we assessed the transcript level of auxin-inducible gene *LATERAL ORGAN BOUNDARIES DOMAIN16* (*MtLBD16*), belonging to *LOB-DOMAIN PROTEIN* family, which is a marker of an onset of lateral root organogenesis (Schiessl et al., 2019). We found that *MtLBD16* mRNA accumulation is enhanced in the *mtabcg40* roots compared to the WT control (Figure 6D).

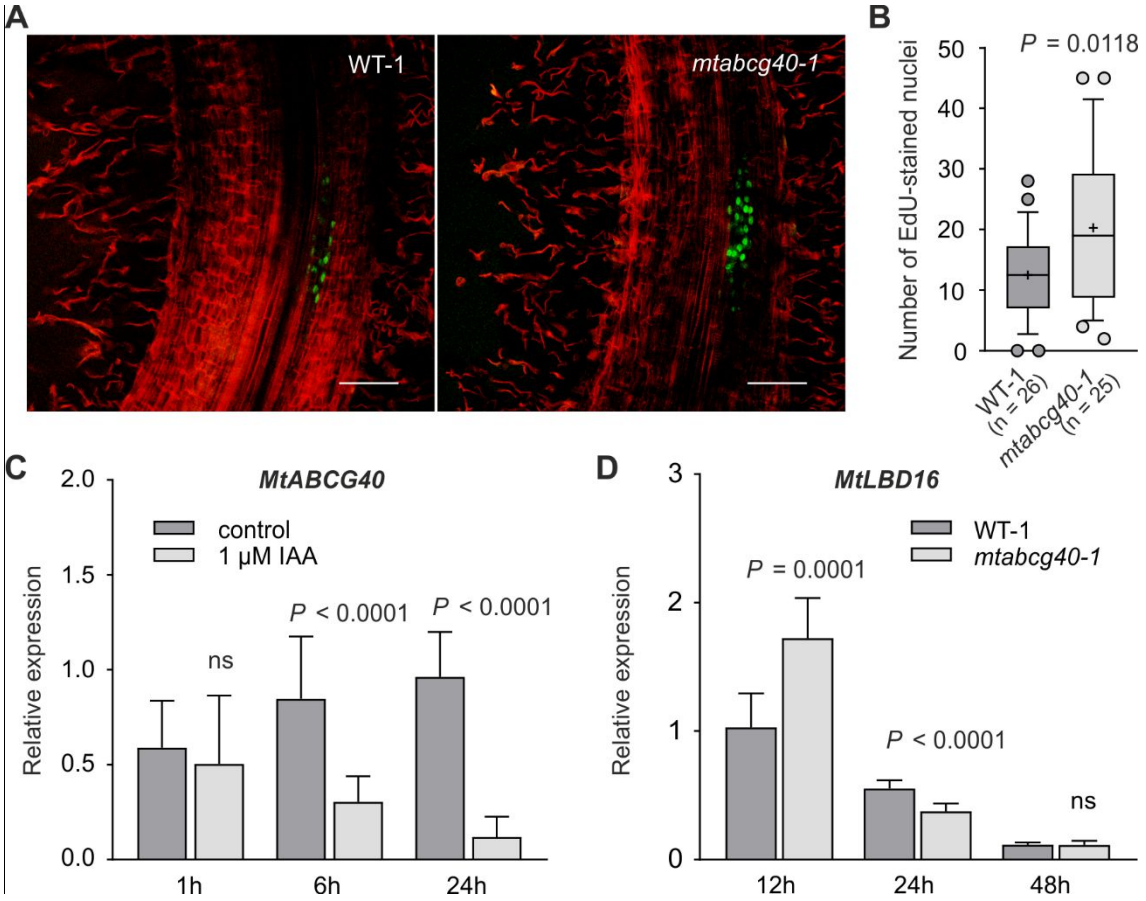

Figure 6. Mutation of *MtABCG40* accelerates cell division within lateral root primordium. A and B, Comparison of cell division rate within lateral root primordium between WT-1 and the *mtabcg40-1* mutant. Optical sections of lateral root primordium 12 hours post induction (hpi) by gravitropic stimulation. Red propidium iodide demarks cell walls and green EdU-labeled nuclei DNA replication. Scale bars: 100 µm (A). Comparison of the number of EdU-stained nuclei within lateral root primordium between WT-1 and the *mtabcg40-1* mutant; n represents the number of individual plants obtained from two independent experiments; for each box-and-whiskers plot: the central black line represents the median; '+' represents the mean; the box extends from the 25th to 75th percentiles; the whiskers are drawn down to the 10th percentile and up to the 90th. Points below and above the whiskers are drawn as individual dots (B). C, Transcript level of *MtABCG40* in roots that were mock-treated or treated with 1 µM indole-3-acetic acid (IAA). D, Expression analysis of *MtLBD16* in *mtabcg40-1* and WT-1. Transcript levels measured by quantitative real-time PCR and normalized to *actin*; data represent the mean ± SD of three independent biological experiments and three technical repeats (C and D). Significant differences from the control plants determined by two-tailed Student's t-test with Welch correction (B), two-tailed Mann–Whitney test (C) or two-tailed Student's t-test (D); ns, not significant.

MtABCG40 inhibits the initial stages of nodule formation

MtABCG40 is present both in nodules and in the root (Figure 1A). Its promoter activity in nodules was confirmed by an analysis of tissue-specific expression pattern during nodulation (Figure 7A). Transcriptomic data from Schiessl et al. (2019) showed a suppression of *MtABCG40* during the onset of both lateral root and nodule organogenesis (Supplemental Figure S8). Our results showed that this was related to the inhibitory influence of the transporter on lateral root initiation (Figure 6), thus we also examined the role of MtABCG40 in the early

stages of nodulation. We initially assessed the response of *MtABCG40* to Nod factors (NFs). The latter are produced by the bacterial microsymbiont as a part of a chemical dialogue with plant roots in nitrogen-deprived conditions, which initiates nodule formation (Zuanazzi et al., 1998). We inoculated the roots of *M. truncatula* with suspensions of two strains of symbiotic bacteria: *S. meliloti* E65, which constitutively overproduces NFs, and, as a control, *S. meliloti* SL44 which is unable to produce NFs. We found that *MtABCG40* was induced 24 h after inoculation with *S. meliloti* E65 (Figure 7B). To quantify the effect of MtABCG40 on nodulation, we counted the nodule number of *mtabcg40* plants. Both mutant lines (*mtabcg40-1* and *mtabcg40-2*) produced more nodules than their respective wild types, implying that MtABCG40 plays a negative role in nodule formation (Figure 7C). To find out if the transporter affects the initiation of nodule primordia, we used a method of bacterial spot inoculation, in which a droplet of *S. meliloti* suspension was applied onto the susceptible zone (Figure 7D). We detected an enhanced expression of *MtLBD16* in *mtabcg40-1* compared to WT-1 plants (Figure 7E). This finding was associated with a higher number of cells labelled with EdU in the *mtabcg40-1* nodule primordia in comparison to WT-1 (Figure 7, F and G). As in the case of lateral roots, these results imply that MtABCG40 suppresses initial cell divisions in nodule formation.

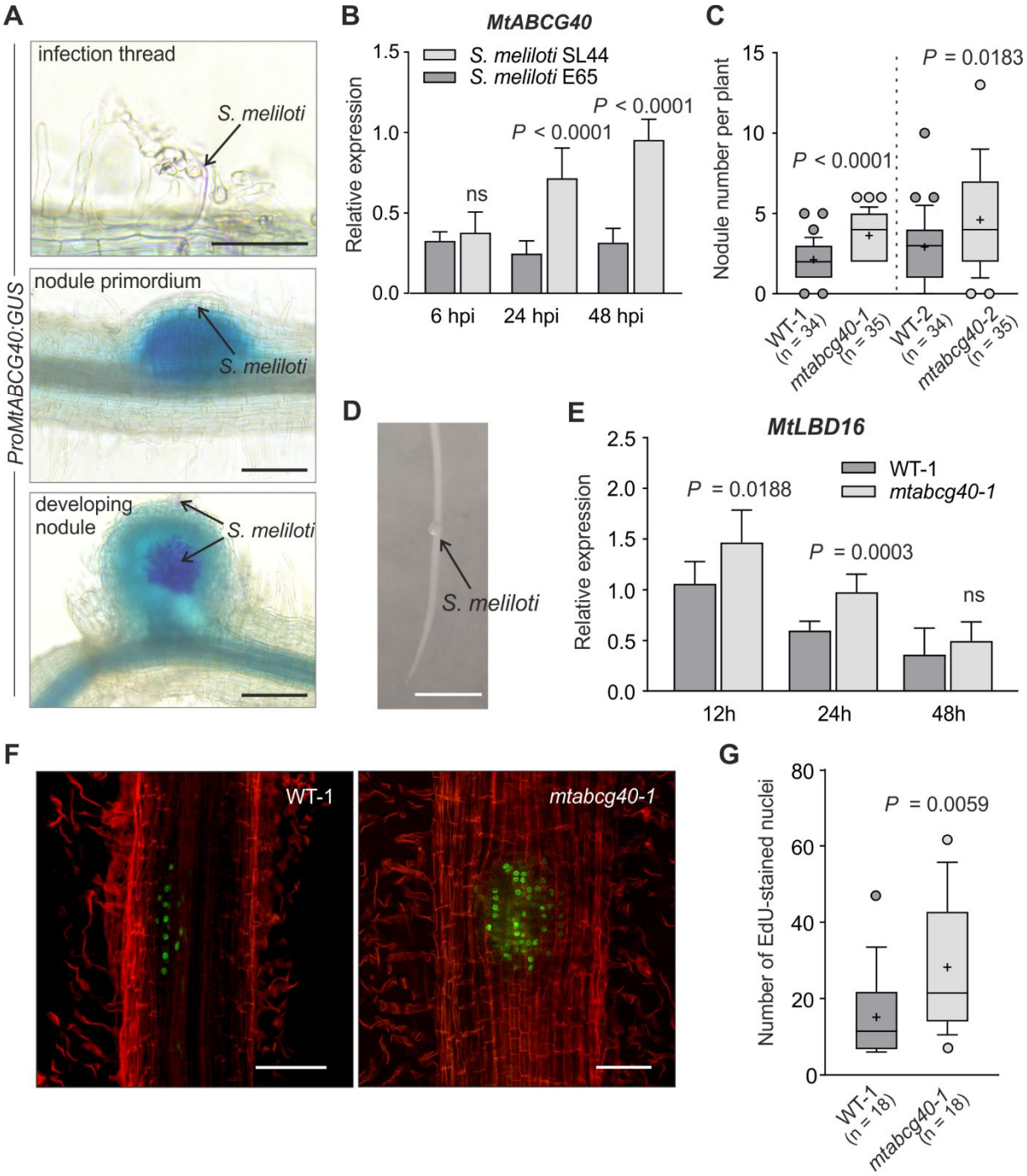

Figure 7. MtABCG40 negatively influences nodule number. A, The tissue-specific expression of *MtABCG40* during nodulation of transgenic roots carrying the *ProMtABCG40:GUS* construct. The pictures show an infection event in the rhizodermis (top), primordium (middle) and a developing nodule (bottom). Double staining using Magenta-Gal and X-Gluc allowed the visualization of the infecting *S. meliloti* in magenta and MtABCG40 expression in blue. The black arrows point at the infection threads or nodule infected cells. Scale bars: 50 µM, 100 µM and 100 µM, respectively. B, Comparison of *MtABCG40* expression in roots flood-inoculated with suspensions of *S. meliloti* E65 (constitutively overproducing Nod factors) and SL44 (unable to produce NFs). C, Nodule number formed on control (WT) and mutant (*mtabcg40*) plants 21 days after *S. meliloti* 1021 wild-type strain inoculation. For each box-and-whiskers plot: the central black line represents the median; '+' represents the mean; the box extends from the 25th to 75th percentiles; the whiskers are drawn down to the 10th percentile and up to the 90th. Points below and above the whiskers are drawn as individual dots; n represents the number of individual plants obtained from two independent biological experiments. D-G, Analysis of auxin response and cell division rate in spot-inoculated fragments during early stages of nodulation. A photo

of root spot-inoculated with a drop of *S. meliloti* suspension. Scale bar: 0.5 cm (D). Expression analysis of *MtLBD16* in *mtabcg40* and WT-1 roots (E). F and G, Comparison of the cell division rate within lateral root primordia between *mtabcg40-1* and WT-1. Optical sections of nodule primordia 12 hours post inoculation (hpi). Red propidium iodide demarks cell walls and green EdU-labeled nuclei DNA replication (F). Comparison of the number of EdU-stained nuclei within nodule primordium between WT-1 and *mtabcg40-1* mutant (G). Transcript levels measured by quantitative real-time PCR and normalized to *actin* (B and E). n represents the number of individual plants obtained from two (G) or three (C) independent experiments; for each box-and-whiskers plot: the central black line represents the median; '+' represents the mean; the box extends from the 25th to 75th percentiles; the whiskers are drawn down to the 10th percentile and up to the 90th. Points below and above the whiskers are drawn as individual dots (C and G). Significant differences from the control plants determined by two-tailed Mann–Whitney test (B, C, E and G).

DISCUSSION

Root development is a postembryonic process that is highly plastic in responding to fluctuations of nutrient levels in the environment. The change in root morphology is tightly linked to the activity of RAMs and to the formation of lateral roots, both controlled by hormonal crosstalk (Jia and von Wiren, 2020). Our studies suggested that under nitrogen shortage MtABCG40 is involved in the negative control of lateral root density (Figure 1B and 2A). The latter results from an enhanced elongation of the primary root and a decrease of lateral root number (Figure 2, B and C).

It was previously shown that an increase of the primary root length under low nitrogen results from a reduction of CK levels in the root, and is a consequence of enhanced cell division in the RAM, their subsequent elongation, as well as their slower transition to differentiation (Dello Ioio et al., 2007; Nehnevajova et al., 2019; Wang et al., 2020). Interestingly, earlier studies suggested that CK metabolism and translocation is modulated by nitrogen status (Takei et al., 2002). We found that nitrogen shortage leads to locally increased expression of *LOG* genes in the root (Figure 4A), which is expected to promote the conversion of inactive CKs into their free, biologically active forms (Kurakawa et al., 2007). Notably, expression of *MtLOG3* was observed in the root cap (Figure 4D), a site of *de novo* CK synthesis that is known to strongly influence RAM activity in N-sufficient conditions (Tsugeki and Fedoroff, 1999; Aloni et al., 2005). The lack of an inhibitory effect of the root cap-derived CKs on RAM activity and overall root elongation under N-deficiency suggests the existence of a mechanism for reducing the sensitivity of RAM meristematic cells to this hormone. PM localization of the MtABCG40, functioning as an importer of active forms of CK and expressed in RAM cells (Figure 3 and 4C), implies that the activity of this transporter may lower the concentration of apoplastic CKs in the root meristematic zone. As a consequence, CK free bases would bind less frequently to

the PM cytokinin receptors of RAM cells, the presence of which was recently confirmed by Kubiasova et al., (2020). This could reduce CK inhibitory effect on RAM development (Figure 8). In this scenario, the role of MtABCG40 would resemble that of Arabidopsis PUP14 (Zurcher et al., 2016). This statement is strengthened by the lack of changes in the total amount of active CKs and the increased expression of *MtRR4*, a primary response marker for CK (Gonzalez-Rizzo et al., 2006) in the RAMs of *mtabcg40* in comparison to WT (Figure 5, C and D). Moreover, the potential increase of free base CKs in the apoplast of *mtabcg40* was also reflected by a shorter root tip in relation to WT (Figure 5, A and B) and led to shorter roots in the mutants (Figure 2B), which was also reported for mutants in PUP14 (Zurcher et al., 2016). Interestingly, the increase in stimulation of RAM cells by active CKs in *mtabcg40* roots was associated with an accumulation of IAA (Figure 5E) and an elevation of auxin signaling (Figure 5F). This could be due to an enhanced auxin biosynthesis, which was shown to take place after treatment with CKs (Jones et al., 2010; Yan et al., 2017), and/or a described disruptive influence of CKs on polar auxin transport (Marhavy et al., 2011). Interestingly, auxin accumulation in the reduced RAMs of *mtabcg40* is consistent with the observation of root shortening after an exogenous IAA treatment (Supplemental Figure S9).

Apart from the regulation of the primary root length, CK also influences lateral root development (Werner et al., 2001; To et al., 2004; Gonzalez-Rizzo et al., 2006). It was shown that CKs negatively impact auxin signaling in lateral root founder cells (LRFCs), thus perturbing their transition to mitosis and suppressing the subsequent development of lateral root primordia (Laplaze et al., 2007). Of note, CK signaling is repressed in LRFC-forming xylem pole pericycle, in contrast to neighboring cells. In the latter, CK-driven suppression of LR initiation is unhampered, thereby controlling lateral root spacing around the root radius (Chang et al., 2015). The increased number of lateral roots in *mtabcg40* (Figure 2C) implies a possible regulatory role of MtABCG40 in the control of auxin signaling during lateral root formation. The idea that MtABCG40 may influence LRFCs in *M. truncatula* is also reinforced by transcriptomic data obtained by Schiessl et al. (2019). These show, apart from an induction of auxin-responsive genes, which positively influence lateral root initiation (e.g. *MtLBD16*), suppression of *MtABCG40*, as a putative negative regulator of this process (Supplemental Figure S8). In line with this, we observed an increase of the pace of cell divisions (Figure 6, A and B) and a simultaneous enhancement of *MtLBD16* expression (Figure 6D) in *mtabcg40* roots after lateral root induction using gravi-stimulation. Of note, the aforementioned role of MtABCG40 in RAM together with suggested PM localization of CK receptors in meristematic cells does not explain the effect that this transporter exerts on the lateral root initiation. This is

most likely due to a potential lack of PM receptors for CKs in these differentiated stele cells (Kubiasova et al., 2020). The presence of MtABCG40 predominantly inside the root stele (Figure 4C) suggests its involvement in the inhibition of lateral root initiation, which takes place in the pericycle, endodermis and inner cortex (Herrbach et al., 2014). Since xylem vessels are the source of CKs (Osugi et al., 2017), we propose that this influence could be due to an import of CK free bases from the xylem apoplast into cells of the root stele. Moreover, prior to import by MtABCG40, the inactive CKs in the xylem should first be converted to their free bases by LOG enzymes, which are present in the root vasculature and whose activity also reduces lateral root number (Kurakawa et al., 2007) (Figure 4, B and D and Supplemental Figure S6). It can thus be proposed that during inhibition of lateral root initiation, import of active CKs into the stele cells by MtABCG40 facilitates an overall outward translocation of the hormone from the vascular vessels to the apoplast that surrounds LRFCs (Figure 8). Accordingly, the observations of an increased *MtLBD16* expression and cell number in primordia of gravistimulated *mtabcg40* roots (Figure 6) were likely the aftermath of an inhibitory effect that MtABCG40 triggers during LRFCs initial divisions rather than LR outgrowth. On the contrary, MtABCG40 function in developing lateral root primordia may resemble the cells of the RAM due to their meristematic character, in which case they may feature PM-localized CK receptors (Kubiasova et al., 2020).

Nodulation and lateral root formation are often considered as competing processes. This is partially due to the contrary phenotypes observed for CK-related mutants, as observed for the CK receptor *cre1* from *M. truncatula*, which features an increased nodulation and decreased lateral root formation (Gonzalez-Rizzo et al., 2006; Laffont et al., 2015). The difference likely results from the spatial changes in *MtCre1* expression from the pericycle and endodermis to the cortex which occur during the transition of the root from the non-symbiotic to symbiotic state (Boivin et al., 2016; Jardinaud et al., 2016). The latter involves production of cortical CKs as an early prerequisite for nodule initiation (Murray et al., 2007; Reid et al., 2017). Thereby, mutation of CK receptors and transporters in the cortex inhibits nodulation (Gonzalez-Rizzo et al., 2006; Jarzyniak et al., 2021). In the non-symbiotic state, MtABCG40 exerts a negative impact on lateral root number (Figure 2C) similar to MtCre1 (Gonzalez-Rizzo et al., 2006). Since both genes are expressed in the vascular bundle under non-symbiotic conditions (Boivin et al., 2016) (Figure 4C), their corresponding phenotypes imply an existence of a mechanism which utilizes vascular CKs and suppresses lateral root development. The role of CKs in this process is further supported by an increase of lateral root number after root tip removal (Lloret et al., 1988), which results in elimination of a CK source in the root and, consequently, in the xylem vessels (Aloni et al., 2006). Interestingly, root tip removal also leads to an increase of

nodule numbers (Nutman, 1952), which suggests that this vascular regulatory mechanism affects both organs in the same way (Figure 8). Notably, we observed an increased number of nodules, in addition to more lateral roots, in *mtabcg40* plants (Figure 7C). Mutation in *MtABCG40* also resulted in a larger number of cell divisions (Figure 7, F and G) and an increased expression of the auxin-responsive gene, *MtLBD16* (Figure 7E) in the mutant nodule primordia. Importantly, the vascular pattern of *MtABCG40* expression did not extend to cortical in response to symbiotic bacteria (Figure 7A). Moreover, *MtABCG40* was not induced quickly after bacterial inoculation (6h), but at later time points (Figure 7B). This suggests that MtABCG40 is unlikely to be involvement in early CK signaling which promotes nodulation (Reid et al., 2017), as MtCre1 or MtABCG40 paralogue, MtABCG56 (Gonzalez-Rizzo et al., 2006; Jarzyniak et al., 2021). Taken together, our results demonstrate an existence of a CK-dependent inhibitory mechanism which suppresses the initiation of nodules and lateral root formation (Figure 8). Thus, MtABCG40 integrates well into the recently suggested developmental overlaps between these two processes (Schiessl et al., 2019).

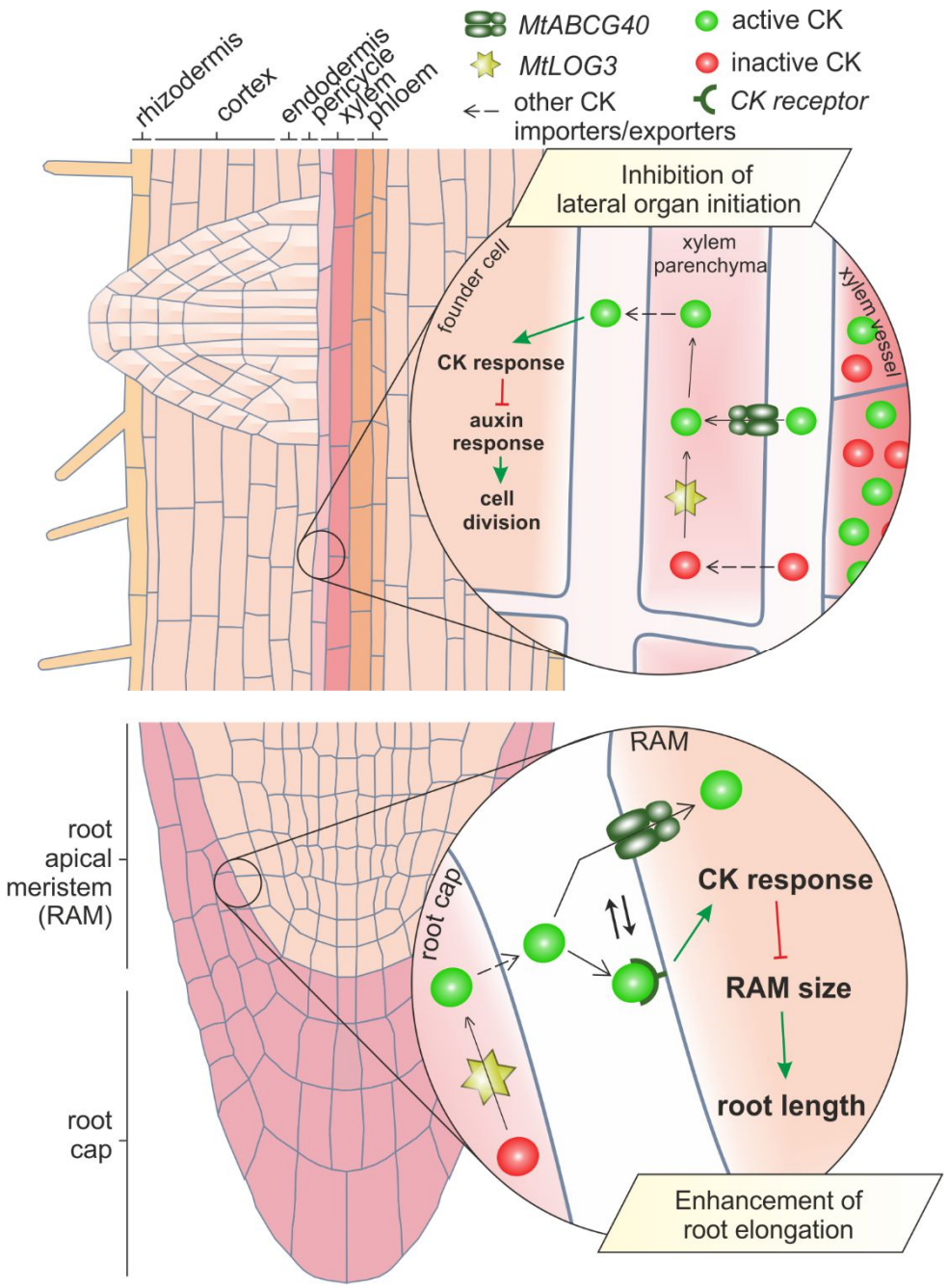

Figure 8. Working model for the MtABCG40 functions in the negative control of lateral root density and nodule number in *Medicago truncatula*. In the root vascular bundles, the root cap-biosynthesized CKs, both biologically active and inactive, are translocated through the xylem vessels towards the shoot, due to the transpiration stream (Aloni et al., 2005). In the nitrogen-depleted environment, active CKs are imported from the apoplast surrounding the vessels to the neighboring stele parenchyma cells by MtABCG40. The latter contributes to the more distant translocation of the hormone to the cells of pericycle, endodermis and inner cortex, which are known to give birth to lateral roots and nodules in *M. truncatula*, suppressing their initial divisions by an inhibition of auxin response (Herrbach et al., 2014; Xiao et al., 2014). Concomitantly, for the acquisition of the inhibitory character, inactive CKs have to be firstly transformed by the enzyme encoded by *MtLOG3*, also expressed in the root vascular bundle, to their active forms. In the root tip, root cap-synthesized inactive CKs (Aloni et al., 2005) are transformed to their active forms by an enzyme encoded by *MtLOG3*. Its expression is induced in the root cap under nitrogen deprivation. For the reduction of the sensitivity of root apical meristem (RAM) to CK, which drives root elongation in these conditions, active CKs are imported into RAM cells from the apoplast by a plasma membrane (PM) transporter, MtABCG40. Thereby, the hormone binds to the

plasma membrane CK receptors less frequently, which suppresses its characteristic outcomes, like the negative influence on the RAM size (Dello Ioio et al., 2007). This active CK pool, produced under nitrogen depletion, together with the inactive forms, is then translocated due to the transpiration stream (Aloni et al., 2005) to the lateral root and nodule-forming areas to inhibit their initiation, which translates to an increase of their spacing on the root surface.

MATERIALS AND METHODS

Plant materials, growth conditions, and treatments

M. truncatula Tnt1 retrotransposon insertion mutant lines, namely NF21323 (*mtabcg40-1*) and NF17891 (*mtabcg40-2*) were obtained from the Noble Research Institute. The presence of the respective insertions was confirmed using polymerase chain reaction (PCR) with *Tnt1*- and gene-specific primers (Supplemental Table S1A). The level of *MtABCG40* expression in homozygous plants was verified using quantitative reverse transcription PCR (RT–qPCR) with gene-specific primers (Supplemental Table S1A).

The seeds of *M. truncatula* Jemalong A17, R108, R108/DR5:GUS stable transgenic plants and *mtabcg40* plants were scarified with 96% sulfuric acid for 10 min, stratified on 0.8% agar plates for 3 days at 4°C and germinated overnight at 21°C. The seedlings were then grown in growth chambers under a 16 h light/8 h dark regime, at 22°C and 50%–60% relative humidity.

Rhizobial strains, namely *S. meliloti* 1021 (wild-type strain), S. *meliloti* SL44 (1021 strain with deletion in the nod genes *ΔnodD1ABC*), *S. meliloti* E65 (A2101/pE65; 1021 strain containing pE65 plasmid that constitutively expresses the *nodD3* gene) and *S. meliloti* Rm1021/pXLGD4 (1021 strain containing plasmid that constitutively expresses the lacZ gene) were used for the inoculation of *M. truncatula*. Bacteria were grown in Bergensen's modified medium (BMM) (Rolfe et al., 1980) containing appropriate antibiotics or 3 μM luteolin (prior to spot-inoculation assays).

For lateral root density measurement, seedlings after germination (ABA and 6-BAP gradients), 1-week-old seedlings (IAA gradient) or 1-week-old composite plants (*MtABCG40* and *MtLOG3* RNAi silencing) grown on full-strength Fähraeus medium were transferred directly onto modified Fähraeus (Barker et al., 2006) agar plates not supplemented with nitrogen (here referred to as 0 mM NH_4NO_3), with different NH_4NO_3 concentrations or full-strength Fähraeus agar plates with varying hormone contents, depending on the type of experiment. The plants were grown for one (IAA gradient), two (ABA, BAP gradients) or three (NH_4NO_3 gradient) weeks, after which the root measurements were taken. Lateral root density was calculated by dividing the number of first order lateral roots by the length of primary root.

If specified, the root samples were collected and immediately frozen for expression analyses. Phenotype analyses were performed on ≥28 (28-74) roots per condition in three independent experimental repetitions. Roots from three plants were pooled for each condition in qRT-PCR analyses, in three biological replicates.

For the expression analyses in RAM, root apical fragments of mutant (*mtabcg40-1*) and corresponding WT plants grown for 10 days on modified Fähraeus agar plates not supplemented with nitrogen were collected. Three independent replicates were performed with ~20 RAMs collected per sample.

For iP, *tZ* and IAA treatments, 7-day-old *M. truncatula* seedlings grown on solid half-strength Murashige and Skoog medium (½ MS; M5524, Sigma-Aldrich) were transferred onto fresh ½ MS medium supplemented with 1 µM of an appropriate hormone, dissolved in NaOH or the equal volume of NaOH (mock). For expression analyses, roots were collected and immediately frozen after 1, 6, and 24 h of treatment. Three independent replicates for each time point were performed with three roots collected per sample.

For *S. meliloti* inoculation assays, seedlings after germination or 3-week-old composite plants grown on full-strength Fähraeus medium were transferred directly onto modified Fähraeus agar plates not supplemented with nitrogen (for assessment of nodule number, expression analyses and EdU staining) or into pots (0.5 l) containing vermiculite/perlite (3:2, v/v) substrate and supplemented with N-free Fähraeus medium, twice a week (GUS and infection thread staining). For assessments of nodule number, roots of respective 4-day-old plants were flood-inoculated with 200 µl of *S. meliloti* 1021 strain (OD_{600} =0.01) each and nodule numbers were counted 21 days post inoculation (dpi). For expression analyses with *S. meliloti* SL44 (1021 strain with deletion in the nod genes *ΔnodD1ABC*) and E65 (1021 strain containing pE65 plasmid that constitutively expresses the *nodD3* gene) roots of 4-day-old Jemalong A17 plants were flood-inoculated with 200 µl of bacterial suspension (OD_{600} =0.01). Root samples were then collected and immediately frozen for expression analyses at the specified time points. For spot-inoculation assays, a 0.5 µl droplet of *S. meliloti* 2011 strain (OD_{600}=0.02) was applied on the root susceptible zone (where the root hairs appear and still elongate) of each of 3-day-old seedlings. 8-12 root fragments (2-3 mm each) comprising the spot-inoculated area were collected 12, 24, and 48 h after an application of a droplet and immediately frozen for expression analyses. Three independent biological repeats were performed. For analysis of the pace of cell divisions, analogous root fragments were stained with EdU (5-ethynyl-2′-deoxyuridine; Thermo Fisher) and modified pseudo-Schiff propidium iodide (PI), as in the case of gravity-induced lateral root initiation.

For GUS and infection thread staining, 200 ml of *S. meliloti* strain (OD_{600} = 0.01) was poured onto the substrate surface (200 ml/l) containing plants grown for 1 week in N-free conditions. The root material was collected and stained 14 days after inoculation (dai).

Genetic constructs and plant transformation

For the analysis of tissue-specific expression pattern, 2015 bp and 2073 bp fragments upstream of ATG start codon, corresponding to the promoter regions of *MtABCG40* and *MtLOG3*, respectively, were amplified with KOD Hot Start DNA Polymerase (Novagen, Madison, Wisconsin, USA) and cloned into pDONR/Zeo (Thermo Fisher) using Gateway Recombination Cloning Technology (Reece-Hoyes and Walhout, 2018). The obtained entry clone was subsequently recombined with pKGWFS7 destination vector, containing the GUS reporter gene sequence (Karimi et al., 2002). *MtABCG40* and *MtLOG3* promoters were also amplified and cloned through ligation-independent cloning into pPLV04_v2 (*MtABCG40:NLS-GFP*) and pPLV11_v2 (*MtLOG3:NLS-tdTomato*), respectively, both carrying reporter genes tagged with a nuclear localization signal (SV40) (De Rybel et al., 2011).

For subcellular localization and transport experiments, a synthetic and codon-optimized DNA fragment (GenScript, Leiden, Netherlands) referring to a hybrid *MtABCG40* sequence, consisting of 1044 bp of gDNA and 3741 bp of cDNA, was cloned into pMDC43 vector between the SgsI (Asc*I*) and Pac*I* restriction sites (GenScript). Afterward, the 686 bp sequence of Ubi10 promoter from *A. thaliana* (Grefen et al., 2010) was amplified and cloned into the construct (*ProUBI10:GFP-MtABCG40*), replacing the 35S promoter by restriction-ligation, using restriction sites for Pst*I* and BamH*I*.

For RNAi silencing, a 188 bp cDNA fragment of *MtABCG40* 5'UTR or a 200 bp cDNA fragment of *MtLOG3* 3'UTR were amplified with KOD Hot Start DNA Polymerase (Novagen) and cloned into pDONR/Zeo (Thermo Fisher) using Gateway Recombination Cloning Technology. The obtained entry clone was subsequently recombined with pK7GWIWG2(II):DsRED binary vector.

Composite plants with transgenic roots were obtained through *Agrobacterium rhizogenes* Arqua1-mediated transformation, described by (Boisson-Dernier et al., 2001) with modifications. Shortly, the plants after transformation were kept at 20°C on full-strength Fähraeus agar plates containing 1 mM aminoisobutyric acid. After a week, emerged and potentially non-transgenic hairy roots were removed and the plants were transferred onto fresh Fähraeus, full-strength or 0 mM NH_4NO_3, at 23°C for 2-3 weeks to obtain transgenic roots. The identification of transgenic roots was possible due to an antibiotic or DsRed selection,

639 depending on the vector used. At least more than 30 composite plants resulting from two or
640 three independent transformations per construct were obtained.
641
642 **MtABCG40 localisation and Transport assays**
643 For tobacco localization experiments, *ProUBI10:GFP-MtABCG40* was expressed in *N.*
644 *benthamiana* leaf tissue by *Agrobacterium tumefaciens*-mediated leaf infiltration as described
645 previously (Henrichs et al. 2012)**.** For confocal laser scanning microscopy, a Leica SP5 confocal
646 laser microscope was used and confocal settings were set to record the emission of GFP
647 (excitation 488 nm, emission 500–550 nm) and FM4-64 (excitation 543 nm, emission 580-640
648 nm).
649 For protoplast transport assays, protoplasts were prepared from Agrobacterium-
650 transfected *N. benthamiana* leaves and [^{14}C]*t*Z and [^{3}H]IAA export was quantified as described
651 previously (Henrichs et al. 2012). In short, tobacco mesophyll protoplasts were prepared 4 days
652 after Agrobacterium-mediated transfection of *ProUBI10:GFP-MtABCG40* or the empty vector
653 control. Equal protoplast loading was achieved by diffusion and export was determined by
654 separating protoplasts and supernatants by silicon oil centrifugation. Relative export from
655 protoplasts is calculated from exported radioactivity into the supernatant as follows:
656 (radioactivity in the supernatant at time t = x min.) - (radioactivity in the supernatant at time t
657 = 0)) * (100%)/ (radioactivity in the supernatant at t = 0 min.). In some cases, relative import
658 into tobacco protoplasts was determined by separating protoplasts and supernatants by silicon
659 oil centrifugation. [^{14}C]*t*Z loading was calculated from imported radioactivity into protoplasts
660 as follows: (radioactivity in the protoplasts at time t = x min.) - (radioactivity in the protoplasts
661 at time t = 0)) * (100%)/ (radioactivity in the protoplasts at t = 0 min.); presented are mean
662 values from 4 independent transfections and protoplasts preparations.
663
664 **Microscopic observations and staining**
665 Transgenic roots carrying a GUS (*β-glucuronidase*) reporter gene were stained using 5-bromo-
666 4-chloro-3-indolyl-β-D-glucuronide (Gallagher, 1992) with an addition of 20% methanol
667 (Kosugi et al., 1990). *M. truncatula* roots inoculated with *S. meliloti* 1021 (pXLGD4) strain
668 were stained using 5-bromo-6-chloro-3-indolyl-β-d-galactopyranoside (Magenta-Gal),
669 according to the protocol described previously by Jarzyniak et al. (2021).
670 For measurement of RAM size, roots of 10-day-old plants grown on full-strength
671 Fähraeus agar plates were collected and immediately subjected to the modified pseudo-Schiff
672 propidium iodide (PI) staining of cell walls described by (Schiessl et al., 2019). Next, the

material was cleared by incubation in chloral hydrate solution and mounted in Hoyer's medium according to the protocol of (Truernit et al., 2008). The length of RAMs was measured as a distance between a stem cell niche and the elongation/differentiation zone (EDZ), indicated by an onset of elongation of the second layer of cortical cells (Shen et al., 2019). The cells were visualized under Leica TCS SP5 laser scanning confocal microscope using Nomarski. The material was analyzed in two independent experiments, with more than 14 RAMs collected per one repetition.

For gravity-induced lateral root initiation, plants were grown vertically on full-strength Fähraeus agar plates for three days, turned 135° for 12 h to constrain a growth-mediated curvature of the root, and turned back afterward to the initial orientation. Root samples, comprising 10-15 newly created <0.5 cm bents each, were collected 12, 24, and 48 h after onset of lateral root initiation and immediately frozen for expression analyses. Three independent biological repeats were performed. For analysis of the pace of cell divisions, analogous root bents were stained with EdU (5-ethynyl-2′-deoxyuridine; Thermo Fisher) and modified pseudo-Schiff propidium iodide (PI) according to the protocol described by (Schiessl et al., 2019). The samples were subsequently cleared by incubation in chloral hydrate (Sigma-Aldrich) solution and mounted in Hoyer's medium according to the protocol of (Truernit et al., 2008). Microscopic observations were carried out using Leica TCS SP5 laser scanning confocal microscope (Carl Zeiss AG, Oberkochen, Germany) with an excitation filter set at 488 nm and emission filters set to 572–625 nm and 505–600 nm for propidium iodide and EdU, respectively. Finally, the number of EdU-stained nuclei in each of the analyzed root fragments per *mtabcg40-1* and respective WT plants from two independent biological repeats was counted.

Gene expression analyses

The isolation of total RNA from the collected samples was performed with the use of the RNeasy Mini Kit (QIAGEN, Hilden, Germany) according to the manufacturer's instructions. Removal of the DNA from the samples was carried out through a DNase I treatment (QIAGEN). The cDNA was then synthesized with an Omniscript Reverse Transcription (RT) Kit (QIAGEN). Quantitative PCR reactions were carried out in a CFX Connect Real-time PCR detection system (BioRad, Hercules, California, USA) using iTaq Universal SYBR Green Supermix (BioRad) with at least three biological replicates each with three technical repeats. The relative mRNA expression levels were normalized to *Mtactin* and calculated using the ΔΔCt method.

Phytohormone quantification

For CK and auxin quantification, seeds of mutant (*mtabcg40-1, mtabcg40-2*) and corresponding WT plants after germination were transferred onto modified Fähraeus agar plates not supplemented with nitrogen. 50 RAMs of 10-day-old seedlings per sample were collected into sterile high-purity water and lyophilized. Three or two biological replicates per mutant/WT were prepared. Endogenous levels of cytokinin metabolites and IAA were determined by LC-MS/MS methods (Svacinova et al., 2012; Pencik et al., 2018). 50 RAMs were homogenized and extracted in 0.5 ml of modified Bieleski buffer (60% MeOH, 10% HCOOH and 30% H_2O) with added stable isotope-labeled internal standards (0.25 pmol of CK bases, ribosides, N-glucosides, 0.5 pmol of CK O-glucosides and nucleotides, and 5 pmol of [$^{13}C_6$]IAA per sample). Phytohormones were determined using an ultra-high performance liquid chromatography-electrospray tandem mass spectrometry (an Acquity UPLC I-Class System coupled to a Xevo TQ-S MS, all from Waters) using stable isotope-labelled internal standards as a reference.

Statistical analyses

Statistical analyses were performed using the GraphPad Prism software (v.8.0). The normality assumption was verified on residuals by the usage of the Shapiro–Wilk normality test. The normal distribution of residuals from each group was analyzed separately. If the normality assumptions were met, parametric tests (i.e. two-tailed Student's t-test, two-tailed Student's t-test with Welch correction, one-way ANOVA with a post hoc Tukey's multiple comparison test) were applied. If the normality assumptions were not met, non-parametric tests (i.e. two-tailed Mann–Whitney test, Kruskal-Wallis test with a post hoc Dunn's multiple comparison test) were applied.

Accession numbers

The sequence data from this article can be found in Phytozome v13 database under the following accession numbers: *MtABCG40* (Medtr7g098300), *MtLOG1* (Medtr7g101290), *MtLOG2* (Medtr1g064260), *MtLOG3* (Medtr1g057020), *MtLOG-like 1* (Medtr1g015830), *MtLOG-like 2* (Medtr2g094790), *MtLOG-like 3* (Medtr3g113710), *MtLOG-like 4* (Medtr4g058740), *MtLBD16* (Medtr7g096530), *MtRR4* (Medtr5g036480), *Mtactin* (Medtr3g095530).

SUPPLEMENTAL DATA

Supplemental Figure S1. Main root length and lateral root number of *Medicago truncatula* at different concentrations of NH_4NO_3.

Supplemental Figure S2. Characterization of NF21323 (*mtabcg40-1*) and NF17891 (*mtabcg40-2*) mutant lines of MtABCG40 used in the study.

Supplemental Figure S3. Lateral root density of control (WT) an mutant (*mtabcg40*) plants grown on media supplemented with 1 mM NH_4NO_3.

Supplemental Figure S4. Phylogenetic tree of full-size ABCG proteins from *Arabidopsis thaliana* and *Medicago truncatula* showing the close relation of MtABCG40 and MtABCG56.

Supplemental Figure S5. A heat map showing a decline in *AtLOG7* expression in the root pericycle triggered within 48 h after an addition of 5 mM NH_4NO_3 to the nitrogen-depleted (0.3 mM NH_4NO_3) media.

Supplemental Figure S6. Effect of *MtLOG3* and *MtABCG40* RNAi silencing on hairy root morphology under nitrogen starvation.

Supplemental Figure S7. Schematic representation of lateral root induction using gravitropic stimulation.

Supplemental Figure S8. Changes of expression of *MtABCG40* and *MtLBD16*, an auxin-responsive gene, during lateral root and nodule formation in the gravitropic stimulation and spot-inoculation assays, respectively.

Supplemental Figure S9. Primary root length of *Medicago truncatula* upon 1 µM indole-3-acetic acid (IAA) in comparison to non-treated control.

Supplemental Table S1. List of primers used in the study.

ACKNOWLEDGEMENTS

We are thankful to J. D. Murray and E. Martinoia for critical reading; T. Ostrowski and G. Framski for the provision of chemicals; D. Weijers for the pPLV11_v02 binary vector; A. van Zeijl for *S. meliloti* 2011/pMH682; B.G. Rolfe for *S. meliloti* 1021/pHC60 strain; M.J. Barnett for *S. meliloti* A2101/pE65 strain; Sharon R. Long for *S. meliloti* Rm1021/pXLGD4.

Funding

This work was supported by the National Science Centre, Poland (grant no. 2015/19/B/NZ9/03548 to M.J.), the Swiss National Funds (project 310030_197563 to M.G.), and the ERDF project "Plants as a tool for sustainable global development" (No. CZ.02.1.01/0.0/0.0/16_019/0000827 to O.N.).

Competing Interests: The authors declare no competing interests.

Contributions

M.J. devised and supervised the project. T.J. and M.J. designed the experiments and interpreted the results. T.J. performed the majority of the experiments. T.J. performed phenotypic characterization of plants, including mutants and silenced material. J.B. and T.J. performed microscopic observations (RAM length, EdU staining, promoter analyses). T.J., A.P. and K.J. generated the plasmids and performed qRT-PCR analyses. T.J. and A.P. performed plant transformation. M.G. and J.X. designed and performed transport experiments. F.R.I performed subcellular localization in *N. benthamiana* leaf epidermal cells. O.N., W.B.L. and L.P. conducted quantification of endogenous cytokinins and auxins. T.J. conducted most of the statistical analyses. T.J. and J.B. prepared figures. T.J. proposed a working model. T.J., M.J. and J.B. wrote the manuscript with the help of co-authors. All authors saw and commented on the manuscript.

The author responsible for distribution of materials integral to the findings presented in this article in accordance with the policy described in the Instructions for Authors (https://academic.oup.com/plcell/pages/General-Instructions) is: Michał Jasiński (jasinski@ibch.poznan.pl).

REFERENCES

Aloni R, Aloni E, Langhans M, Ullrich CI (2006) Role of cytokinin and auxin in shaping root architecture: regulating vascular differentiation, lateral root initiation, root apical dominance and root gravitropism. Ann Bot 97: 883-893

Aloni R, Langhans M, Aloni E, Dreieicher E, Ullrich CI (2005) Root-synthesized cytokinin in Arabidopsis is distributed in the shoot by the transpiration stream. J Exp Bot 56: 1535-1544

Aubry E, Dinant S, Vilaine F, Bellini C, Le Hir R (2019) Lateral transport of organic and inorganic solutes. Plants 8

Banasiak J, Borghi L, Stec N, Martinoia E, Jasinski M (2020) The full-size ABCG transporter of *Medicago truncatula* is involved in strigolactone secretion, affecting arbuscular mycorrhiza. Front Plant Sci 11: 18

Banasiak J, Jasiński M (2014) Defence, symbiosis and ABCG transporters. *In* M Geisler, ed, Plant ABC Transporters, Vol 22. Springer International Publishing, Cham, pp 163-184

Bargmann BO, Vanneste S, Krouk G, Nawy T, Efroni I, Shani E, Choe G, Friml J, Bergmann DC, Estelle M, Birnbaum KD (2013) A map of cell type-specific auxin responses. Mol Syst Biol 9: 688

Barker DG, Pfaff T, Moreau D, Groves E, Ruffel S, Lepetit M, Whitehand S, Maillet F, Nair, R.,, Journet E (2006) Growing *M. truncatula*: choice of substrates and growth conditions. *In* UJ Mathesius, EP., L Sumner, eds, The *Medicago truncatula* handbook. Samuel Roberts Noble Foundation, Ardmore

816 Boisson-Dernier A, Chabaud M, Garcia F, Becard G, Rosenberg C, Barker DG (2001) *Agrobacterium*
817 *rhizogenes*-transformed roots of *Medicago truncatula* for the study of nitrogen-fixing and
818 endomycorrhizal symbiotic associations. Molecular Plant-Microbe Interactions 14: 695-700
819 Boivin S, Kazmierczak T, Brault M, Wen JQ, Gamas P, Mysore KS, Frugier F (2016) Different
820 cytokinin histidine kinase receptors regulate nodule initiation as well as later nodule
821 developmental stages in *Medicago truncatula*. Plant Cell Environ 39: 2198-2209
822 Chang L, Ramireddy E, Schmulling T (2015) Cytokinin as a positional cue regulating lateral root
823 spacing in Arabidopsis. J Exp Bot 66: 4759-4768
824 Cornelius S, Traub M, Bernard C, Salzig C, Lang P, Mohlmann T (2012) Nucleoside transport across
825 the plasma membrane mediated by equilibrative nucleoside transporter 3 influences metabolism
826 of Arabidopsis seedlings. Plant Biol 14: 696-705
827 De Rybel B, van den Berg W, Lokerse A, Liao CY, van Mourik H, Moller B, Peris CL, Weijers D (2011)
828 A versatile set of ligation-independent cloning vectors for functional studies in plants. Plant
829 Physiol 156: 1292-1299
830 Dello Ioio R, Linhares FS, Scacchi E, Casamitjana-Martinez E, Heidstra R, Costantino P, Sabatini S
831 (2007) Cytokinins determine Arabidopsis root-meristem size by controlling cell differentiation.
832 Curr Biol 17: 678-682
833 Dello Ioio R, Nakamura K, Moubayidin L, Perilli S, Taniguchi M, Morita MT, Aoyama T, Costantino
834 P, Sabatini S (2008) A genetic framework for the control of cell division and differentiation in
835 the root meristem. Science 322: 1380-1384
836 Gallagher SR (1992) GUS protocols: using the GUS gene as a reporter of gene expression. Academic
837 Press., San Diego
838 Geisler M, Blakeslee JJ, Bouchard R, Lee OR, Vincenzetti V, Bandyopadhyay A, Titapiwatanakun B,
839 Peer WA, Bailly A, Richards EL, Ejenda KFK, Smith AP, Baroux C, Grossniklaus U, Muller
840 A, Hrycyna CA, Dudler R, Murphy AS, Martinoia E (2005) Cellular efflux of auxin catalyzed
841 by the Arabidopsis MDR/PGP transporter AtPGP1. Plant J 44: 179-194
842 Gonzalez-Rizzo S, Crespi M, Frugier F (2006) The *Medicago truncatula* CRE1 cytokinin receptor
843 regulates lateral root development and early symbiotic interaction with *Sinorhizobium meliloti*.
844 Plant Cell 18: 2680-2693
845 Grefen C, Donald N, Hashimoto K, Kudla J, Schumacher K, Blatt MR (2010) A ubiquitin-10 promoter-
846 based vector set for fluorescent protein tagging facilitates temporal stability and native protein
847 distribution in transient and stable expression studies. Plant J 64: 355-365
848 Gu JF, Li ZK, Mao YQ, Struik PC, Zhang H, Liu LJ, Wang ZQ, Yang JC (2018) Roles of nitrogen and
849 cytokinin signals in root and shoot communications in maximizing of plant productivity and
850 their agronomic applications. Plant Science 274: 320-331
851 Herrbach V, Rembliere C, Gough C, Bensmihen S (2014) Lateral root formation and patterning in
852 *Medicago truncatula*. J Plant Physiol 171: 301-310
853 Jardinaud MF, Boivin S, Rodde N, Catrice O, Kisiala A, Lepage A, Moreau S, Roux B, Cottret L, Sallet
854 E, Brault M, Emery RJ, Gouzy J, Frugier F, Gamas P (2016) A laser dissection-RNAseq analysis
855 highlights the activation of cytokinin pathways by Nod factors in the *Medicago truncatula* root
856 epidermis. Plant Physiol 171: 2256-2276
857 Jarzyniak K, Banasiak J, Jamruszka T, Pawela A, Di Donato M, Novak O, Geisler M, Jasinski M (2021)
858 Early stages of legume-rhizobia symbiosis are controlled by ABCG-mediated transport of active
859 cytokinins. Nat Plants 7: 428-436
860 Jia Z, von Wiren N (2020) Signaling pathways underlying nitrogen-dependent changes in root system
861 architecture: from model to crop species. J Exp Bot 71: 4393-4404
862 Jones B, Gunneras SA, Petersson SV, Tarkowski P, Graham N, May S, Dolezal K, Sandberg G, Ljung
863 K (2010) Cytokinin regulation of auxin synthesis in Arabidopsis involves a homeostatic
864 feedback loop regulated via auxin and cytokinin signal transduction. Plant Cell 22: 2956-2969
865 Kang J, Hwang JU, Lee M, Kim YY, Assmann SM, Martinoia E, Lee Y (2010) PDR-type ABC
866 transporter mediates cellular uptake of the phytohormone abscisic acid. Proc Natl Acad Sci USA
867 107: 2355-2360
868 Karimi M, Inze D, Depicker A (2002) GATEWAY vectors for *Agrobacterium*-mediated plant
869 transformation. Trends Plant Sci 7: 193-195
870 Kieber JJ, Schaller GE (2014) Cytokinins. Arabidopsis Book 12: e0168

Ko D, Kang J, Kiba T, Park J, Kojima M, Do J, Kim KY, Kwon M, Endler A, Song WY, Martinoia E, Sakakibara H, Lee Y (2014) Arabidopsis ABCG14 is essential for the root-to-shoot translocation of cytokinin. Proc Natl Acad Sci U S A 111: 7150-7155

Korobova A, Kuluev B, Mohlmann T, Veselov D, Kudoyarova G (2021) Limitation of cytokinin export to the shoots by nucleoside transporter ENT3 and its linkage with root elongation in Arabidopsis. Cells 10

Kosugi S, Ohashi Y, Nakajima K, Arai Y (1990) An improved assay for Beta-Glucuronidase in transformed-cells - methanol almost completely suppresses a putative endogenous Beta-Glucuronidase activity. Plant Science 70: 133-140

Kretzschmar T, Kohlen W, Sasse J, Borghi L, Schlegel M, Bachelier JB, Reinhardt D, Bours R, Bouwmeester HJ, Martinoia E (2012) A petunia ABC protein controls strigolactone-dependent symbiotic signalling and branching. Nature 483: 341-344

Kubiasova K, Montesinos JC, Samajova O, Nisler J, Mik V, Semeradova H, Plihalova L, Novak O, Marhavy P, Cavallari N, Zalabak D, Berka K, Dolezal K, Galuszka P, Samaj J, Strnad M, Benkova E, Plihal O, Spichal L (2020) Cytokinin fluoroprobe reveals multiple sites of cytokinin perception at plasma membrane and endoplasmic reticulum. Nat Commun 11

Kurakawa T, Ueda N, Maekawa M, Kobayashi K, Kojima M, Nagato Y, Sakakibara H, Kyozuka J (2007) Direct control of shoot meristem activity by a cytokinin-activating enzyme. Nature 445: 652-655

Laffont C, Rey T, Andre O, Novero M, Kazmierczak T, Debelle F, Bonfante P, Jacquet C, Frugier F (2015) The CRE1 cytokinin pathway is differentially recruited depending on *Medicago truncatula* root environments and negatively regulates resistance to a pathogen. Plos One 10

Laplaze L, Benkova E, Casimiro I, Maes L, Vanneste S, Swarup R, Weijers D, Calvo V, Parizot B, Herrera-Rodriguez MB, Offringa R, Graham N, Doumas P, Friml J, Bogusz D, Beeckman T, Bennett M (2007) Cytokinins act directly on lateral root founder cells to inhibit root initiation. Plant Cell 19: 3889-3900

Lefevre F, Boutry M (2018) Towards identification of the substrates of ATP-binding cassette transporters. Plant Physiol 178: 18-39

Lima JE, Kojima S, Takahashi H, von Wiren N (2010) Ammonium triggers lateral root branching in *Arabidopsis* in an AMMONIUM TRANSPORTER1;3-dependent manner. Plant Cell 22: 3621-3633

Lloret PG, Casero PJ, Navascues J, Pulgarin A (1988) The effects of removal of the root-tip on lateral root distribution in adventitious roots of anion. New Phytol 110: 143-149

Lopez-Bucio J, Cruz-Ramirez A, Herrera-Estrella L (2003) The role of nutrient availability in regulating root architecture. Curr Opin Plant Biol 6: 280-287

Marhavy P, Bielach A, Abas L, Abuzeineh A, Duclercq J, Tanaka H, Parezova M, Petrasek J, Friml J, Kleine-Vehn J, Benkova E (2011) Cytokinin modulates endocytic trafficking of PIN1 auxin efflux carrier to control plant organogenesis. Dev Cell 21: 796-804

Miri M, Janakirama P, Huebert T, Ross L, McDowell T, Orosz K, Markmann K, Szczyglowski K (2019) Inside out: root cortex-localized LHK1 cytokinin receptor limits epidermal infection of *Lotus japonicus* roots by *Mesorhizobium loti*. New Phytol 222: 1523-1537

Mortier V, Wasson A, Jaworek P, De Keyser A, Decroos M, Holsters M, Tarkowski P, Mathesius U, Goormachtig S (2014) Role of *LONELY GUY* genes in indeterminate nodulation on *Medicago truncatula*. New Phytol 202: 582-593

Murray JD, Karas BJ, Sato S, Tabata S, Amyot L, Szczyglowski K (2007) A cytokinin perception mutant colonized by Rhizobium in the absence of nodule organogenesis. Science 315: 101-104

Nehnevajova E, Ramireddy E, Stolz A, Gerdemann-Knorck M, Novak O, Strnad M, Schmulling T (2019) Root enhancement in cytokinin-deficient oilseed rape causes leaf mineral enrichment, increases the chlorophyll concentration under nutrient limitation and enhances the phytoremediation capacity. BMC Plant Biol 19: 83

Nutman PS (1952) Studies on the physiology of nodule formation. Experiments on the excision of root-tips and nodules. Ann Bot 16: 79-&

Oldroyd GE, Murray JD, Poole PS, Downie JA (2011) The rules of engagement in the legume-rhizobial symbiosis. Annu Rev Genet 45: 119-144

Osugi A, Kojima M, Takebayashi Y, Ueda N, Kiba T, Sakakibara H (2017) Systemic transport of trans-zeatin and its precursor have differing roles in Arabidopsis shoots. Nat Plants 3: 17112

Pawela A, Banasiak J, Biala W, Martinoia E, Jasinski M (2019) MtABCG20 is an ABA exporter influencing root morphology and seed germination of *Medicago truncatula*. Plant J 98: 511-523

Pencik A, Casanova-Saez R, Pilarova V, Zukauskaite A, Pinto R, Micol JL, Ljung K, Novak O (2018) Ultra-rapid auxin metabolite profiling for high-throughput mutant screening in Arabidopsis. Journal of Experimental Botany 69: 2569-2579

Postma JA, Dathe A, Lynch JP (2014) The optimal lateral root branching density for maize depends on nitrogen and phosphorus availability. Plant Physiol 166: 590-602

Reece-Hoyes JS, Walhout AJM (2018) Gateway Recombinational Cloning. Cold Spring Harb Protoc 2018

Reid D, Nadzieja M, Novak O, Heckmann AB, Sandal N, Stougaard J (2017) Cytokinin biosynthesis promotes cortical cell responses during nodule development. Plant Physiol 175: 361-375

Rolfe BG, Gresshoff PM, Shine J (1980) Rapid screening for symbiotic mutants of rhizobium and white clover. Plant Sci Lett 19: 277-284

Romanov GA, Lomin SN, Schmulling T (2018) Cytokinin signaling: from the ER or from the PM? That is the question! New Phytol 218: 41-53

Sasaki T, Suzaki T, Soyano T, Kojima M, Sakakibara H, Kawaguchi M (2014) Shoot-derived cytokinins systemically regulate root nodulation. Nat Commun 5: 4983

Schiessl K, Lilley JLS, Lee T, Tamvakis I, Kohlen W, Bailey PC, Thomas A, Luptak J, Ramakrishnan K, Carpenter MD, Mysore KS, Wen J, Ahnert S, Grieneisen VA, Oldroyd GED (2019) NODULE INCEPTION recruits the lateral root developmental program for symbiotic nodule organogenesis in *Medicago truncatula*. Curr Biol 29: 3657-3668 e3655

Shen D, Kulikova O, Guhl K, Franssen H, Kohlen W, Bisseling T, Geurts R (2019) The *Medicago truncatula* nodule identity gene *MtNOOT1* is required for coordinated apical-basal development of the root. BMC Plant Biol 19: 571

Svacinova J, Novak O, Plackova L, Lenobel R, Holik J, Strnad M, Dolezal K (2012) A new approach for cytokinin isolation from Arabidopsis tissues using miniaturized purification: pipette tip solid-phase extraction. Plant Methods 8

Takei K, Takahashi T, Sugiyama T, Yamaya T, Sakakibara H (2002) Multiple routes communicating nitrogen availability from roots to shoots: a signal transduction pathway mediated by cytokinin. J Exp Bot 53: 971-977

Tessi TM, Brumm S, Winklbauer E, Schumacher B, Pettinari G, Lescano I, Gonzalez CA, Wanke D, Maurino VG, Harter K, Desimone M (2021) Arabidopsis AZG2 transports cytokinins in vivo and regulates lateral root emergence. New Phytol 229: 979-993

To JP, Haberer G, Ferreira FJ, Deruere J, Mason MG, Schaller GE, Alonso JM, Ecker JR, Kieber JJ (2004) Type-A Arabidopsis response regulators are partially redundant negative regulators of cytokinin signaling. Plant Cell 16: 658-671

Traub M, Florchinger M, Piecuch J, Kunz HH, Weise-Steinmetz A, Deitmer JW, Neuhaus HE, Mohlmann T (2007) The fluorouridine insensitive 1 (*fur1*) mutant is defective in equilibrative nucleoside transporter 3 (ENT3), and thus represents an important pyrimidine nucleoside uptake system in *Arabidopsis thaliana*. Plant J 49: 855-864

Truernit E, Bauby H, Dubreucq B, Grandjean O, Runions J, Barthelemy J, Palauqui JC (2008) High-resolution whole-mount imaging of three-dimensional tissue organization and gene expression enables the study of Phloem development and structure in *Arabidopsis*. Plant Cell 20: 1494-1503

Tsugeki R, Fedoroff NV (1999) Genetic ablation of root cap cells in Arabidopsis. Proc Natl Acad Sci USA 96: 12941-12946

van Zeijl A, Op den Camp RH, Deinum EE, Charnikhova T, Franssen H, Op den Camp HJ, Bouwmeester H, Kohlen W, Bisseling T, Geurts R (2015) Rhizobium lipo-chitooligosaccharide signaling triggers accumulation of cytokinins in *Medicago truncatula* roots. Mol Plant 8: 1213-1226

Walker L, Boddington C, Jenkins D, Wang Y, Gronlund JT, Hulsmans J, Kumar S, Patel D, Moore JD, Carter A, Samavedam S, Bonomo G, Hersh DS, Coruzzi GM, Burroughs NJ, Gifford ML (2017)

Changes in gene expression in space and time orchestrate environmentally mediated shaping of root architecture. Plant Cell 29: 2393-2412

Wang Q, Zhu Y, Zou X, Li F, Zhang J, Kang Z, Li X, Yin C, Lin Y (2020) Nitrogen deficiency-induced decrease in cytokinins content promotes rice seminal root growth by promoting root meristem cell proliferation and cell elongation. Cells 9

Werner T, Motyka V, Strnad M, Schmulling T (2001) Regulation of plant growth by cytokinin. Proc Natl Acad Sci USA 98: 10487-10492

Xiao TT, Schilderink S, Moling S, Deinum EE, Kondorosi E, Franssen H, Kulikova O, Niebel A, Bisseling T (2014) Fate map of *Medicago truncatula* root nodules. Development 141: 3517-3528

Yan ZW, Liu X, Ljung K, Li SN, Zhao WY, Yang F, Wang ML, Tao Y (2017) Type B response regulators act as central integrators in transcriptional control of the auxin biosynthesis enzyme TAA1. Plant Physiol 175: 1438-1454

Zhang KW, Novak OR, Wei ZY, Gou MY, Zhang XB, Yu Y, Yang HJ, Cai YH, Strnad M, Liu CJ (2014) Arabidopsis ABCG14 protein controls the acropetal translocation of root-synthesized cytokinins. Nat Commun 5: 3274

Zhao J, Yu N, Ju M, Fan B, Zhang Y, Zhu E, Zhang M, Zhang K (2019) ABC transporter OsABCG18 controls the shootward transport of cytokinins and grain yield in rice. J Exp Bot 70: 6277-6291

Zurcher E, Liu J, di Donato M, Geisler M, Muller B (2016) Plant development regulated by cytokinin sinks. Science 353: 1027-1030